Kiel University
Christian-Albrechts-Universität zu Kiel

UNIVERSITY OF GOTHENBURG

DEPARTMENT OF PHYSICS

Analysis of directional Mie scattering spectra through optical levitation

Bachelor's thesis in Physics

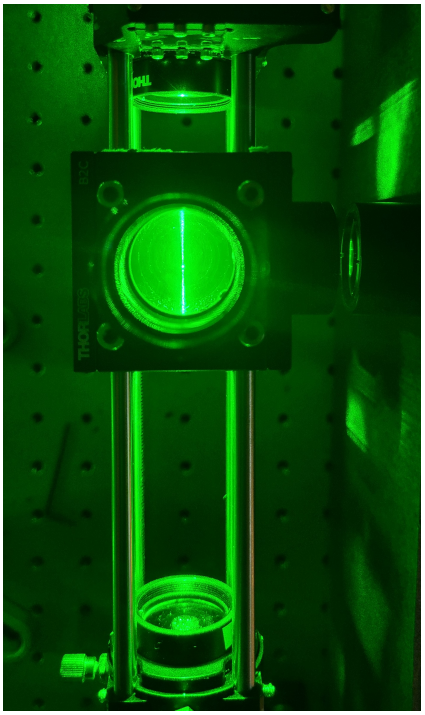

Jolina Pech

Degree project for Bachelor of Science (180 ECTS) with a major in Physics
2023

Analysis of directional Mie scattering spectra trough optical levitation

JOLINA PECH

Supervisor: Javier Tello Marmolejo
Examinator: Martina Ahlberg

UNIVERSITY OF GOTHENBURG

Department of Physics
Research Group of Laser Spectroscopy
Gothenburg, Sweden 2023

Preface

The present thesis was composed and evaluated at the University of Gothenburg, following the institution's rigorous standards. The research was conducted while pursuing academic studies abroad in Sweden through the Erasmus program. This work will serve as a requirement for the attainment of a Bachelor's degree of science from Kiel University.

Acknowledgements

I would like to express my sincere gratitude to my supervisor, Javier, for providing me with this opportunity and for his invaluable support, guidance, and encouragement throughout my thesis. I would also like to thank Dag Hanstorp for welcoming me into the group and making this project possible. My heartfelt thanks go to all the Research Group of Laser Spectroscopy members, especially the other students, for their helpful discussions and support. Finally, I would like to acknowledge the Erasmus program for making this international experience possible.

Abtract

Evaporation rates of droplets have been studied extensively due to their relevance in a variety of fields, such as atmospheric science, materials science, and biology. Optical levitation is a valuable tool for measuring evaporation rates due to their precise manipulation, non-invasive nature, and versatility in studying a wide range of droplet sizes and compositions. The current state-of-the-art technique for measuring the size of an evaporating droplet involves capturing far-field interference patterns on a screen using a camera, leading to imprecise and time-consuming measurements. In this thesis evaporation rates were measured using a recently discovered technique, directional Mie scattering spectra, which offers superior advantages compared to the existing methods. Experiments were conducted to compare the evaporation rates of water, ethanol, and a soap-water solution using both methods. It was found that directional Mie scattering spectra allowed for more precise measurements and enabled the characterization of the complete evaporation process. Specifically, a faster evaporation rate was observed for ethanol, while a slower evaporation rate was observed for the soap-water solution compared to water. The directional Mie scattering method, employed in this research, proves to be an effective tool for precise and comprehensive droplet analysis, offering new opportunities for further investigations in various scientific domains. Overall, this research provides novel insights into the evaporation rates of optically levitated droplets, highlighting the distinct behavior of different liquids and the significance of the directional Mie scattering method. The results enhance the understanding of evaporation processes and offer valuable opportunities for future interdisciplinary investigations.

Contents

1 Introduction

In 1970 Arthur Ashkin pusblished his discovery of a method to trap objects using laser beams [1]. His work was awarded with a Nobel prize in 2018 for groundbreaking inventions in the field of laser physics, specifically optical tweezers and their application to biological systems[2]. When a small dielectric particle with a different refractive index than surrounding medium is placed in a focused laser beam, the particle experiences a force the towards the region of highest intensity of the laser beam. That gradient force depends on the refractive index of the particle, the wavelength of the laser beam, and the shape and size of the particle [3].
The scattering force, on the other hand, arises from the reflection and absorption of photons by the particle. When light is scattered by a particle, the particle experiences a force in the direction of the beam, which can be used to manipulate the position and orientation of the particle. The scattering force is proportional to the scattering cross-section of the particle and the laser beam intensity [4].

Optical levitation has been widely used as a non-contact method for trapping and manipulating micro- and nanometric droplets. It has a range of applicationss, including highly sensitive measurements of the particle's mass and density [5], medical uses that go as far as predicting the airborne transmission of viruses like COVID-19 [6] and in the study of aerosols and atmospheric science: Aerosol particles are widespread in the atmosphere and currently introduce a significant level of uncertainty to climate models [7].

There are two main optical levitation techniques, vertical and counterpropagating. The vertical optical trap involves the use of a focused laser beam to trap a particle in three dimensions, creating a stable equilibrium position for the particle within the trap. It undergoes Brownian motion, exhibiting random fluctuations in its position due to collision with air molecules. The particle is subjected to a potential well, which is formed by the laser beam. The trap stiffness represents the strength of the restoring force that confines the particle in the trap. It is determined by the laser power, the particle size, the refractive index of the medium and of the particle. By monitoring the Brownian motion of the particle, information about the properties of the particle and the surrounding medium can be obtained [8] [9]. In this thesis firstly a vertical optical trap was constructed, the measured potential was plotted and the Brownian motion of a particle in an optical trap was demonstrated.

Secondly, a counterpropagating trap was constructed to was used to study evaporation rates. They are a very relevant droplet property to study in various fields, such as pharmaceuticals and material sciences[10]. The current state of the art to measure the evaporation rates of optically levitated droplets is to measure the far-field diffraction structure with a camera. The video can be used to determine the radius of the trapped droplet: The distance between the maxima of the pattern exhibits an inverse proportionality to the size [11], similar to Young's double slit experiment [12].

Here a different approach of measuring the evaporation rates of droplets is presented based on optical levitation and directional Mie scattering. The phenomenon of Mie scattering has been a subject of extensive research for many years [13]. In this process, a plane wave is scattered by a dielectric small sphere, leading to the whispering galley modes that resonate every λ/n in circumference whereby λ is the used wavelegnth and n the refractive index. Instead of 2D frames of a video that must be analyzed and are limited by the camera's framerate, this technique utilizes a 1D signal of the scattering intensity [11].

This thesis showcases a technique to measure the behavior of the evaporation rates of different liquids, namely water, ethanol and soap-water solution using two different methods: far field interference pattern measurement and directional Mie scattering. The experimental results show that the directional Mie scattering technique is a promising alternative for measuring the evaporation rates of optically levitated droplets, with potential for further applications.

2 Methods

2.1 Experimental set up

Vertical traps and counterpropagating traps are two different configurations of laser beams used to confine and levitate small particles.
A vertical trap uses a single laser beam that is directed upwards. It creates a scattering force on the particle, which balances the downward force of gravity. A counterpropagating trap, also known as a dual-beam trap, utilizes the gradient force generated by two laser beams aligned in opposite directions. The beams intersect near their focus spots, creating a stable trapping region where the particle is held.

2.1.1 Vertical Trap

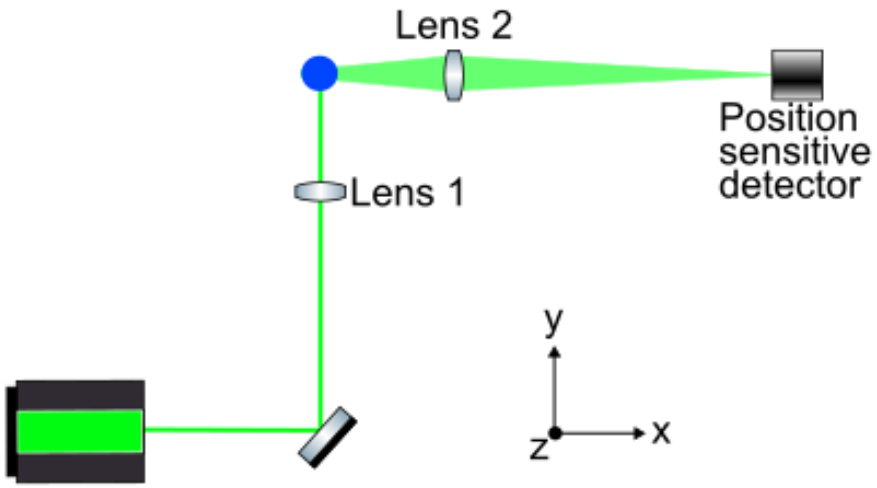

Figure 3: Side view of an optical levitation setup to measure the position of a trapped droplet using scattered light

Figure 3 shows a vertical levitation setup. A continuous wave laser with wavelength $\lambda = 532$ nm and beam diameter $d = 0.9 \pm 0.1$ nm is focused with a lens (Lens 1, focal length $f = 10$ cm) in a chamber. To measure the position, the scattered light is focused and magnified by a lens (Lens 2, $f = 5$ cm) onto a position sensitive detector. The lens equation is used to calculate the magnification of an image produced by a lens. It is given by:

$$\frac{1}{f} = \frac{1}{S_1} + \frac{1}{S_2}, \tag{1}$$

where f is the focal length of the lens, S_1 is the distance between the object and the lens, and S_2 is the distance between the image and the lens. The magnification M of

the image produced by the lens is given by:

$$M = -\frac{S_2}{S_1} = \frac{f}{f - S_1} \tag{2}$$

where M is negative for inverted images and positive for upright images[14].

In the current experimental procedure, silica particles are trapped. They are present in a solution which is deposited onto a glass substrate and subsequently dried. The dried particles are placed on top of the trapping chamber, and gentle tapping or scratching is applied to the glass surface to dispense the particles into the chamber.

The particle experiences a harmonic force that tends to maintain it near a stable equilibrium position. In one dimension, when the particle is displaced slightly from its equilibrium position, a force is exerted on it, as given by the equation

$$F = -k_z(z - z_{eq}), \tag{3}$$

where k_z represents the trap stiffness along the z-axis, and z is the particle's position within the trap, centered at z_{eq}. The resulting trapping potential is a harmonic function, represented by the equation

$$U(z) = \frac{1}{2}k_z(z - z_{eq})^2. \tag{4}$$

As a result of being held in a harmonic trapping potential, the particle's position distribution takes on a Gaussian shape. Following Maxwell statistics, this can be written as

$$\rho(z) = \rho_0 \exp \frac{k_z(z - z_{eq})^2}{2k_B T} \tag{5}$$

from which follows

$$U(z) = -k_B T \ln\Big(\frac{\rho(z)}{\rho_0}\Big), \tag{6}$$

where $\rho(z)$ is the probability distribution along the x dimension, ρ_0 the normalization constant, T the absolute temperature and k_B the Boltzmann constant [15].

2.1.2 Counterpropagating Trap

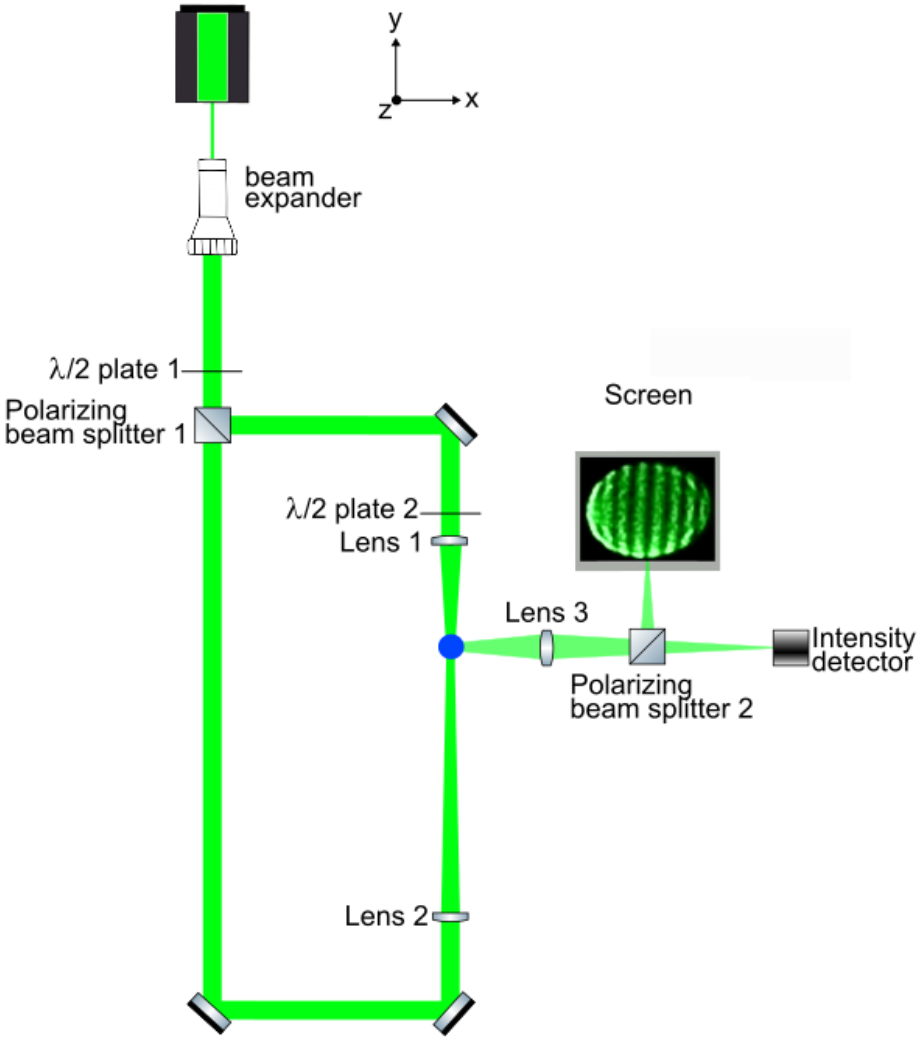

Figure 4: A counterpropagating trap is used to levitate liquid droplets and analyze the evaporation rate using two different methods: recording the far-field interference pattern on a screen and measuring the intensity with a detector.

The setup shown in figure 4 begins with a continuous wave laser beam with wavelength $\lambda = 532$ nm and diameter $d = 0.9 \pm 0.1$ nm, which is initially collimated and directed towards a beam expander which increases the beam size by 10 times to $d = 9 \pm 1$ mm. Next the laser beam passes a $\lambda/2$ plate. Coupled with the polarizing beam splitter it is used to control the relative intensity of the two laser beams.

Both laser beams are then directed towards different lenses ($f_1 = 5$ cm and $f_2 = 10$ cm)

that are aligned to focus the beams to a specific point in a chamber. The focal length of the lenses as well as the magnification of the beam expander are chosen in a way that the beam waist and the size of the objects are comparable. The beam waist is the point along a laser beam's propagation axis where the beam diameter is at its minimum and the intensity at its maximum. It's radius is given by [8]

$$W_0 = \frac{2\lambda}{\pi}\frac{f}{d}, \tag{7}$$

whereby W_0 is the radius of the beam waist and d the diameter of the beam before passing the lenses. Both arms have beam waists of W_{0,f_1}=3,8 µm and W_{0,f_2}=7,5 µm respectively.

A cloud of droplets of the currently used liquid gets dispensed using a ultrasonic nebulizer on top of the chamber. The droplets then merge into the largest drop that the trap could accommodate. Finally, the drop settles and evaporates. The scattered light is collected by a lens ($f_3 = 5$ cm) and then divided by a polarizing beam splitter. The other polarization of the light, I_θ, is directed towards a screen, where the scattered light forms an interference pattern that is captured by a camera. The other I_ϕ polarization is aimed at an intensity detector. For further explanation of the polarization components see 2.2.3.

2.2 Measurements

2.2.1 Position

2D lateral effect sensors accurately measure the position of a light spot projected onto them. They work as variable resistors that distribute photocurrent to determine X and Y position from the four electrodes upon incident light. There are two types of sensors available: duo-lateral and tetra-lateral. While duo-lateral sensors provide higher linearity and accuracy, they are more expensive due to additional resistive layers. On the other hand, tetra-lateral sensors are cheaper to manufacture but have lower linearity as the spot moves away from the center due to the physical location of the anodes. The Thorlabs PDP90A detector shown in figure 5 detector uses a tetra-lateral-type sensor with anodes in the four corners and a reshaped area for improved linearity at a lower cost. The active area is 9x9 mm at the waist and 10mm at the outermost regions. The Δx, Δy, and SUM signals from the PDP90A are decoded using circuitry that implements the following equations:

$$\Delta x = (A + D) - (B + C) \tag{8}$$

$$\Delta y = (A + B) - (C + D) \tag{9}$$

$$SUM = (A + B + C + D). \tag{10}$$

Here, A, B, C, and D are the four electrodes located on the upper surface and formed along each of the four edges. $L_x = 10$ mm and $L_y = 10$ mm are the the wides part of

the area. The axial beam position can be determined with [16]

$$x = \frac{L_x(\Delta x)}{2SUM} \tag{11}$$

$$y = \frac{L_y(\Delta y)}{2SUM} \tag{12}$$

[16]

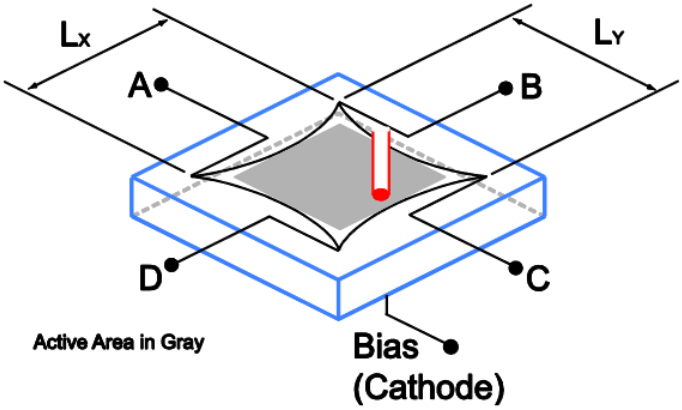

Figure 5: Layout of a Lateral Effect Position Sensor. A, B, C and D are four electrodes on the upper surface, formed along each of the four edges. With permission from [16]

2.2.2 Evaporation rate - interference pattern

The experimental method involves optically levitating a droplet and then projecting the interference pattern shown in figure 7 produced by the droplet onto a screen. The pattern is caused by the interference between the light waves that travel different paths from the droplet to the screen. The trapped particle scatters light mostly at its top and bottom as shown in figure 6, causing constructive and destructive interference at different locations on the screen. The observed interference pattern can be understood in a similar way to the famous double-slit experiment by Young [17]. This fringe pattern is then captured by a camera and analyzed using a computer program. Specifically, the program determines the average distance between the stripes, or intensity maxima, in the interference pattern. Using [11]

$$r = \frac{2d\lambda}{S * (2 + \sqrt{2})} \tag{13}$$

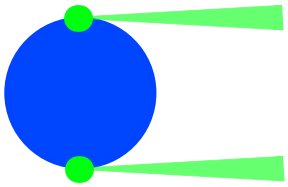

Figure 6: The trapped particle scatters light mostly at its top and bottom, creating an analogy to the double-slit experiment

with radius r, distance to the screen d, the avarage distance between the maxima S and wavelength λ. The radius is plotted over time and fitted with an exponential function. The measurement is restricted to a specific size range where the presence of only one mode precludes further analysis.

Figure 7: The number of interference stripes observed on the screen varies with the size of the droplet: larger droplets exhibit fewer stripes, while smaller droplets display a greater number of stripes. The average distance between the maxima is analyzed and utilized to determine the radius of the droplet.

2.2.3 Evaporation rate - scattering intensity

The first observation of resonances in levitated droplets dates back to 1977, as reported by Ashkin and Dziedzic [18]. A Mie resonance is a phenomenon that occurs when an electromagnetic wave interacts with a spherical object of a size similar to the wavelength of the incident light. In this interaction, the electromagnetic field inside and outside the sphere becomes coupled, leading to the excitation of a resonant mode. This resonance results in the enhancement of the scattered light in a particular direction, which depends on the size and refractive index of the spherical object, as well as the polarization and wavelength of the incident light [19].

Transverse Magnetic (TM) modes and Transverse Electric (TE) modes are two types of electromagnetic waves that can exist in an optical cavity. TM modes are characterized by having a magnetic field that is perpendicular (transverse) to the direction of propagation and no electric field component parallel to the magnetic field. TE modes, on the other hand, have an electric field that is transverse to the direction of propagation and no magnetic field component parallel to the electric field. Both TM and TE modes can exist in a spherical cavity. Due to the use of a polarizing beam splitter 2 in figure 4, only transverse magnetic modes with intensity I_ϕ are present. Having only one polarization in a certain direction filters out many resonance modes and allows to see a directional Mie spectrum. The transverse electric mode with intensity I_θ are used to observe the interference patterns from the last section.

A directional Mie scattering spectrum is made up of Fano combs. They are caused by interference between the scattered light waves, and appear as a series of peaks and dips in the spectrum. This happens when light interacts with a sphere and creates resonances. The resonances occur with every incremental change in circumference of the sphere.[20]

The light travels around inside the sphere and creates constructive interference when the circumference is a multiple of the wavelength inside the material. The phenomenon where light is confined and circulates around the surface of a microstructure with very little attenuation due to total internal reflection is known as a whispering gallery mode. These modes can exist in various structures, including optical cavities, acoustic resonators, and microwave cavities. The name "whispering gallery" refers to the phenomenon of sound waves being able to travel long distances along the curved walls of a circular gallery, allowing two people standing at opposite ends to communicate with each other in a whisper.

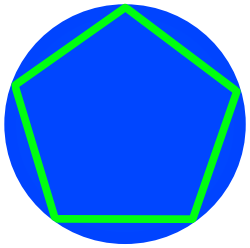

Figure 8: Constructive interference and Whispering Gallery Mode occurs in an optically levitated droplet when the circumference of the droplet is an integer multiple of the wavelength.

The spacing of these peaks provides information about the size change of the droplet. The light wraps around inside the droplet, leading to constructive interference every time the circumference is a multiple of the wavelength inside the material which is λ/n, whereby n is the refractive index of the used liquids. By measuring the distance between these peaks and scaling it with $(\lambda/n)/2\pi$, we can determine the rate at which the droplet's radius changes over time. For water, a new peak appears approximately every 399 nm, for ethanol it occurs around 391 nm, and for soap about 394 nm.

3 Results

3.1 Vertical Trap

Figure 9 (a) depicts a typical trajectory of an optical levitated particle. It moved randomly due to Brownian fluctuations, which resulted in a dynamic equilibrium between the thermal noise and the optical forces. The optical forces continually drove the particle towards the equilibrium position, while the thermal noise continuously pushed it out of the trap.

By making a histogram from trajectory of the particle, the probability density function (PDF) of it's position was determined. The PDF represents the likelihood of finding the particle at a particular position in the trap. A typical PDF for a particle undergoing Brownian motion in a vertical optical trap is shown in figure 9 (b). The width of the PDF is determined by the strength of the Brownian fluctuations and the depth of the optical potential.

For a particle to remain trapped in the optical tweezers, the potential well must be sufficiently deep. This depth is typically measured in units of thermal energy, k_BT, where $k_B = 1,28 * 10^{-23} \frac{J}{K}$ is the Boltzmann constant and T is the absolute temperature. This quantity provides a characteristic energy scale for mesoscopic phenomena. The potential well must be at least a few k_BT deep to effectively confine a particle [15], as shown in figure 9 (c).

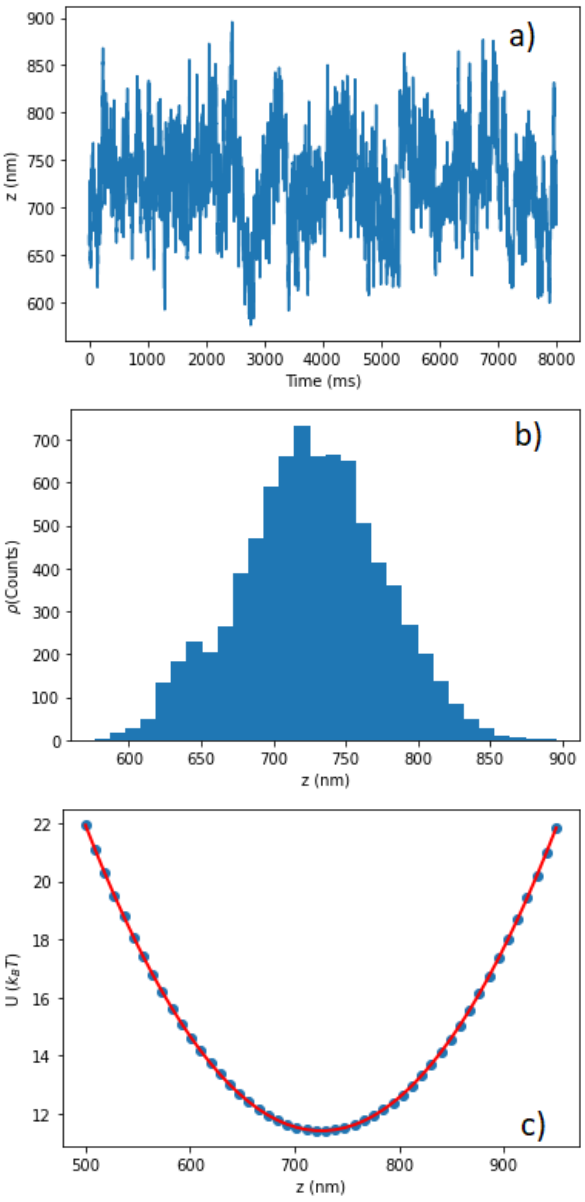

Figure 9: Movement in z-direction of a particle in an vertical trap (a) with it's probability density (b) and the corresponding optical potential (c)

3.2 Counterpropagating Trap

3.2.1 Water

Figure 10 displays the evaporation rate of a water droplet as a function of time, as measured using the far field interference method. The horizontal axis represents time, while the vertical axis shows the radius of the droplet. At the start of the measurement, the evaporation rate was relatively slow and constant, but it increased rapidly over time. The radius could only be measured until 2 µm, since after that only one maxima in the interference pattern were visible and it wasn't possible to calculate the radius.

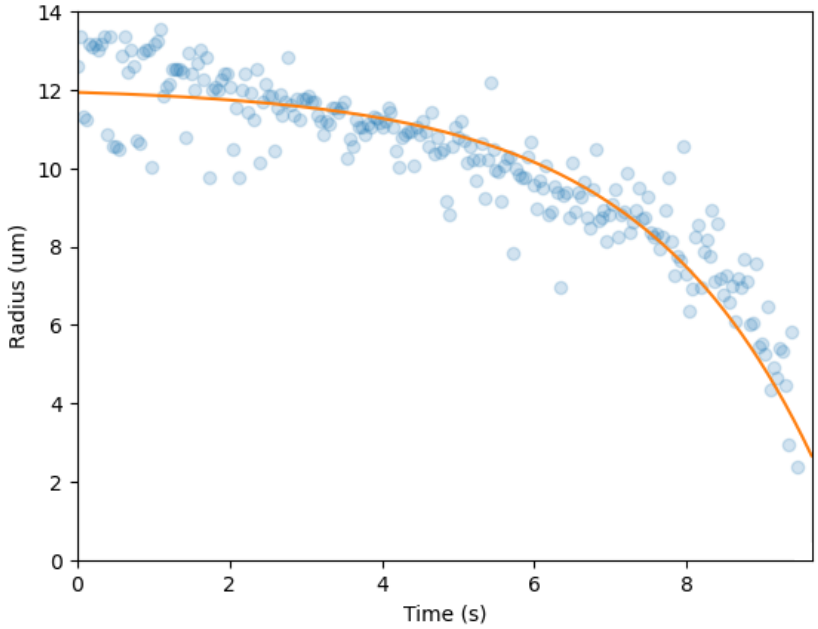

Figure 10: The radius of an evaporating water droplet, fitted with a square root function.

The directional Mie scattering method with Fano combs was used to analyze the evaporation of an optically levitated water droplet. A comb-like structure in the Mie spectrum shown in figure 11 was observed, which was periodic in nature and allowed for the identification of individual resonances. This structure became more prominent as the droplet evaporated, with the resonances becoming narrower and more separated as the droplet size decreased.

Additionally the spectrum is characterized by the presence of three overlapping combs. A combs refers to a set of closely spaced peaks in the spectrum. Here, each comb represents a series of resonances that are equidistant from each other. The overlap implies that there are certain radii where the resonances from two different combs coincide or share

intensity.In contrast to the other method, it was also possible to measure the entire evaporation process with less size limitations. The radius at which the lowest resonance appears, typically around 1 um, sets the limit for that measurements.

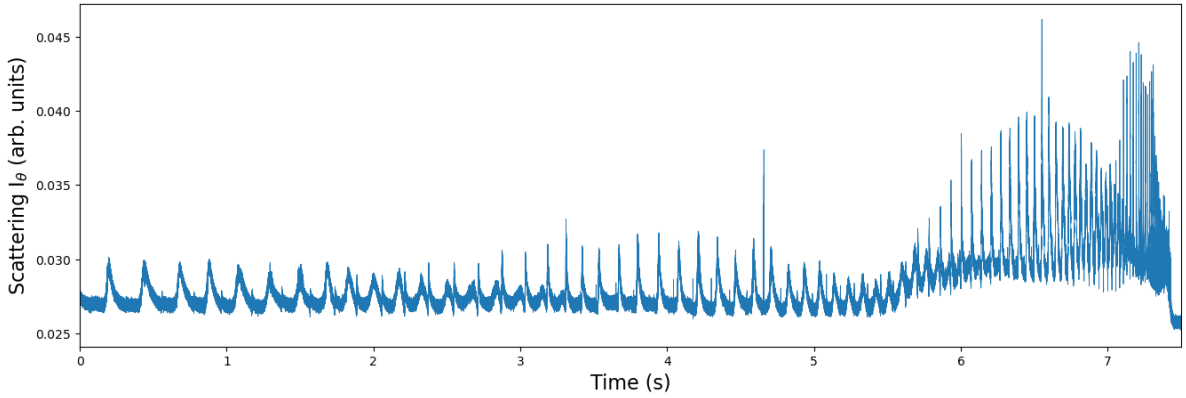

Figure 11: The scattering intensity I_θ of an evaporating water droplet shows a directional Mie spectrum with a fano comb structure.

The evaporation rate is shown in figure 12. It was quantified through the analysis of spectral peaks by measuring the distance between them as described in the method section. The evaporation rate was found to initially increase slowly and then increase more rapidly, which is consistent with the results obtained from the other measurement.

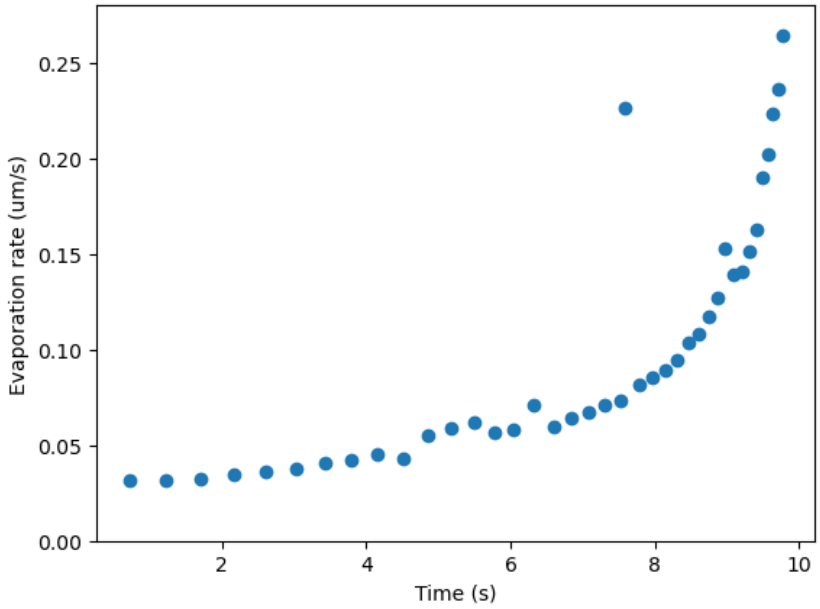

Figure 12: The evaporation rate of a water droplet undergoing evaporation was measured using directional Mie scattering spectra.

3.2.2 Ethanol

The experimental conditions for the measurement of ethanol droplet evaporation rates were the same as for water. The results are shown in figure 13. The main difference observed was that the evaporation rate of the ethanol droplet was faster than that of water, with the ethanol droplet taking about 7 seconds to evaporate to from ca. 12µm to 2 µm, while the water droplet took approximately 10 seconds.

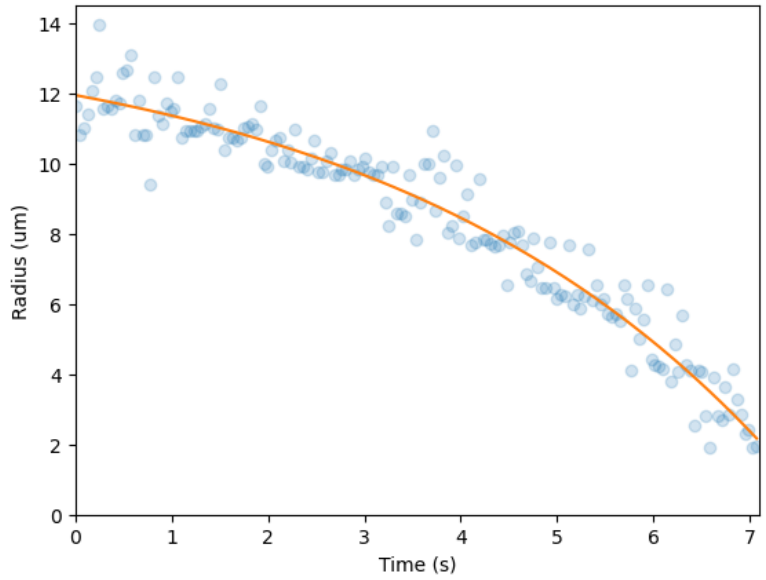

Figure 13: The radius of an evaporating ethanol droplet, fitted with a square root function.

The fano comb structure of the directional Mie scattering in figure 14 is similar to the one with water.

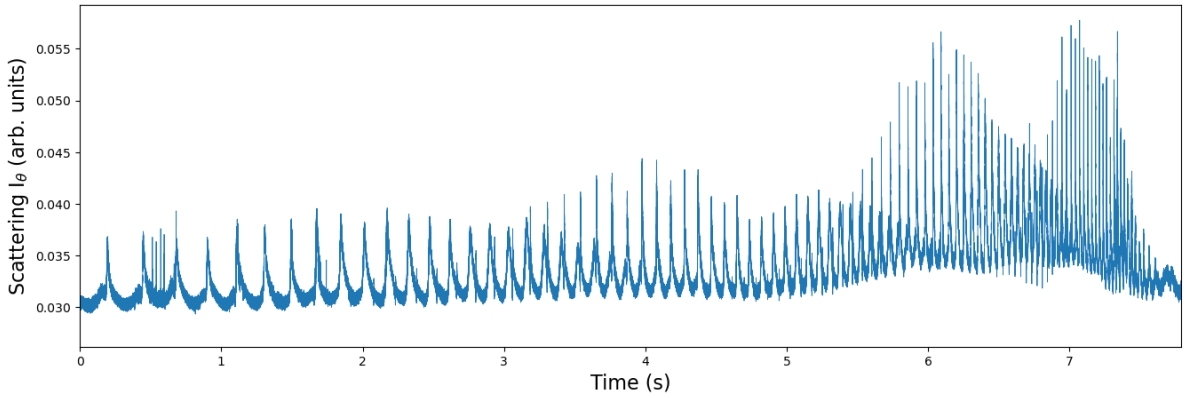

Figure 14: The scattering intensisty I_θ of an evaporating ethanol droplet shows a directional Mie spectrum with a fano comb structure.

The evaporation rate of the optically levitated ethanol droplet is shown in figure 15. It increased more rapidly than that of water: The maximum evaporation rate observed was 0.3 micrometers per second, while for water it was 0.25 micrometers per second. This is consistent with the result that ethanol evaporates faster.

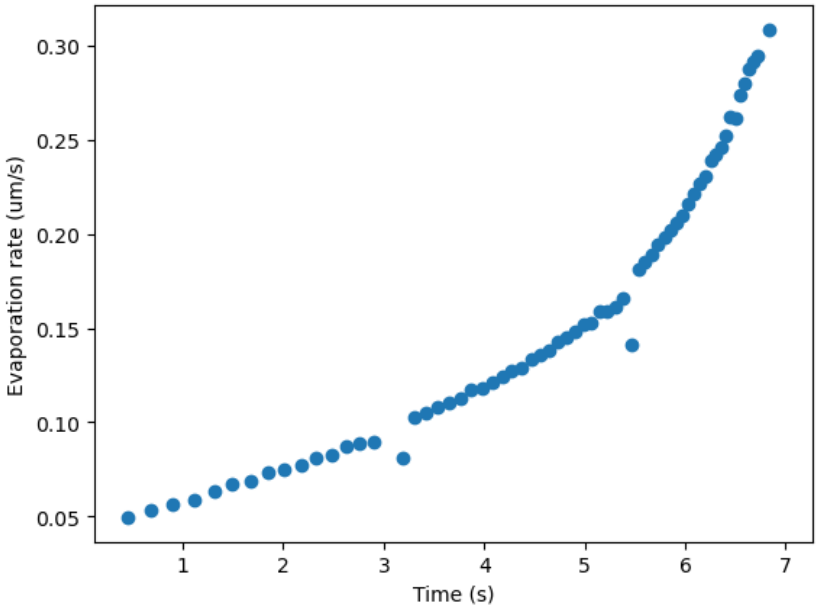

Figure 15: The evaporation rate of a ethanol droplet undergoing evaporation was measured using directional Mie scattering spectra.

3.2.3 Soap-water solution

The used soap solution with 0.1 ml of soap in 100 ml of distilled water was made with regular hand wash soap. Figure 16 shows the evaporation process of a soap water solution droplet under similar conditions as the previous experiments. However, due to the presence of the soap, the droplet evaporated more slowly, taking approximately 20 seconds to evaporate from ca. 11.5 µm to 2 µm.

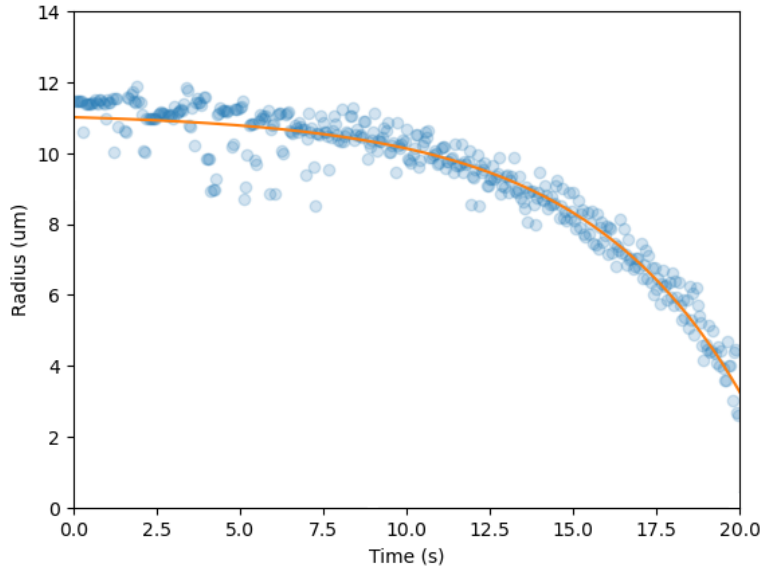

Figure 16: The radius of an evaporating soap-water solution droplet, fitted with a square root function.

The final section of the directional Mie scattering spectrum depicted in figure 17 exhibits a comparable pattern to that observed in the previous measurements.

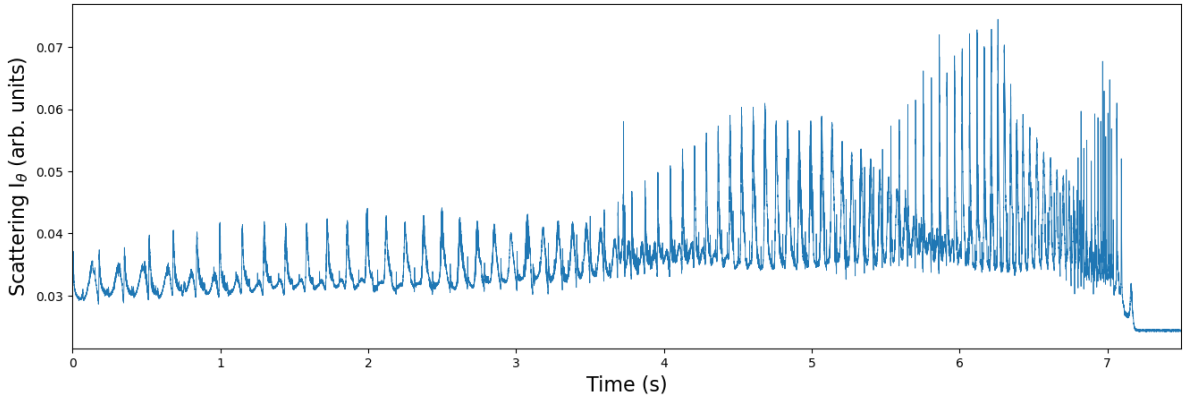

Figure 17: The scattering intensity I_θ of an evaporating soap-water solution droplet shows a directional Mie spectrum with a Fano comb structure.

The evaporation rate shown in figure 18 exhibits an initial slow increase, followed by a gradual acceleration before reaching its maximum value. Instead of a sudden cessation or decline, the evaporation rate displayed a gradual and possibly linear decrease towards the end of the measurement period. The abrupt decrease in the evaporation rate towards the end indicates that when the droplet reached a smaller size, it evaporated at a significantly slower pace until it eventually dissipated completely. The sharp slowdown of the evaporation rate does not show in figure 16 due to the limitations of that measurement method.

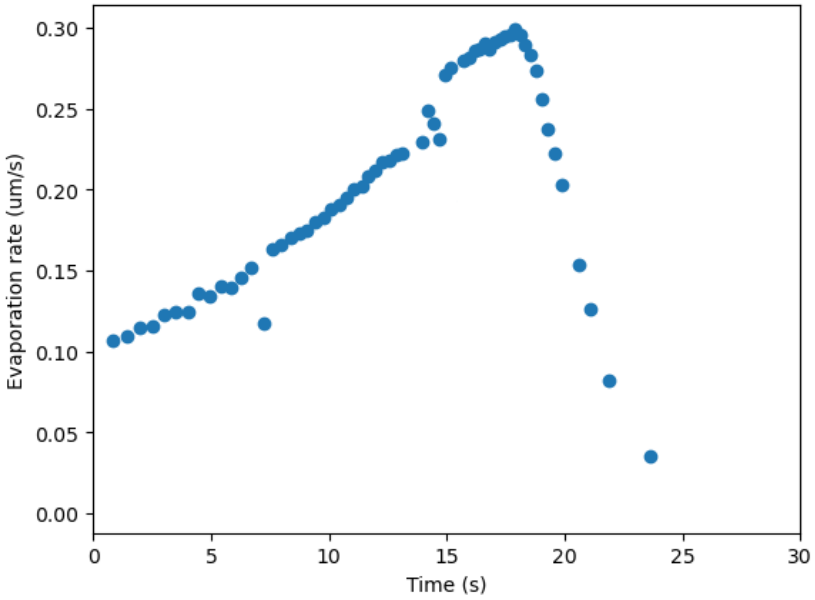

Figure 18: The evaporation rate of a water-water solution droplet undergoing evaporation was measured using directional Mie scattering spectra.

4 Conclusions and discussion

4.1 Vertical trap

In this experimental setup, the vertical trap configuration proved to be an effective method to levitate small particles. The position of the trapped particle was accurately measured using scattered light and a position-sensitive detector. Additionally, the use of silica particles in the experiment demonstrated the suitability of the vertical trap for studying particle dynamics. The harmonic trapping potential provided by the vertical trap allowed for the observation of Gaussian-shaped position distributions, consistent with previous research [15].

4.2 Evaporation rates

The evaporation rates of optically levitated droplets of water, ethanol and soap-water solutions were investigated using interference patterns and directional Mie scattering. The analysis of these evaporation processes provides valuable insights into the behavior of droplets under optical levitation and sheds light on the dynamics of their size reduction.

The results obtained for water align with previous research studies [11]. Ethanol exhibits faster evaporation rate, while soap-water solution evaporates slower compared to water. Water took 10s to evaporate from an initial droplet size of 12 µm to a final size of 2 µm, ethanol took 7s and the soap water solution 20s. The results are the same for both measurement methods.

In the upcoming section, speculative hypotheses and potential explanations for the observed variations in evaporation rates will be presented. Droplets of optically levitated ethanol evaporate faster than water because ethanol a higher vapor pressure than water. The higher vapor pressure of ethanol means that more ethanol molecules will escape from the surface of the droplet into the surrounding air, leading to faster evaporation.

The soap water solution, on the other hand, contains additional components such as surfactants, which can alter the evaporation dynamics. Surfactants tend to reduce the vapor pressure of the liquid, slowing down the evaporation process. Additionally, the presence of soap in the solution can form a thin film or layer on the surface, acting as a barrier that hinders evaporation. This film may take longer to evaporate completely compared to the bulk liquid, leading to the observed longer evaporation time for the soap water solution.

The observed slowdown in the evaporation rate towards the end of the experiment for the soap water solution shown in figure 18, could potentially be attributed to the hypothesis that water evaporates first, leaving behind a higher concentration of soap. The soap, having different properties and a lower vapor pressure compared to water, may evaporate more slowly. Spectroscopy can be employed to investigate this phenomenon by identifying the molecules present in the solution, shedding light on the composition

and behavior of the remaining substances.

While the current research provides valuable insights into the evaporation rates of these droplets using the directional Mie scattering method, further studies are necessary to fully understand the underlying mechanisms and to extend the findings to other liquids and environmental conditions.

4.3 Advantages of Directional Mie Scattering for Measuring Evaporation Rates

The main advantage of using directional Mie scattering for measuring evaporation rates compared to the interference pattern method is the absence of certain limitations. The directional Mie scattering technique provides several benefits that make it a better choice for accurate and efficient measurements.

Firstly, directional Mie scattering allows for a more precise measurement with a more accurate determination of the evaporation rate at different stages of the process. The interference pattern method is limited by the frame rate of the camera used to film the pattern: With a frame rate of 30 frames per second, the measurement yielded 30 data points per second, with each frame captured representing a distinct data point.

Secondly, the analysis of directional Mie scattering spectra is relatively easier and faster compared to interpreting interference patterns: analyzing each video individually for the measurement of evaporation time can be a time-consuming process that involves finding and determining relevant parameters. Directional Mie scattering spectra exhibit distinct features in the form of Fano comb structures, which can be readily analyzed to extract valuable information about the droplet's size and evaporation rate. The clear and well-defined spectral patterns simplify the data analysis process, reducing the time and effort required for interpretation.

Furthermore, the directional Mie scattering method enables the measurement of the end of the evaporation process. Unlike the interference pattern method, which is not able to show the evaporation droplets for droplets below 2 µm, directional Mie scattering allows for continued measurement until the complete evaporation of the droplet. This capability is crucial for capturing the entire evaporation process and obtaining comprehensive data on the evaporation rate, including the behavior of the rate towards the end of the process.

Overall, the directional Mie scattering technique provides significant advantages over the interference pattern method for measuring evaporation rates. It offers more precise measurements, easier and faster data analysis and the ability to capture the complete evaporation process, including the measurement of the end of evaporation. These

advantages make directional Mie scattering a superior choice for accurately studying and characterizing the evaporation dynamics of optically levitated droplets.

References

[1] Arthur Ashkin and JM Dziedzic. Optical levitation by radiation pressure. *Applied Physics Letters*, **19**(8):283–285, 1971.

[2] The nobel prize in physics 2018, https://www.nobelprize.org/prizes/physics/2018/summary/, visited 23.02.2023.

[3] Ryota Omori, Tamiki Kobayashi, and Atsuyuki Suzuki. Observation of a single-beam gradient-force optical trap for dielectric particles in air. *Optics letters*, 22(11):816–818, 1997.

[4] Yasuhiro Harada and Toshimitsu Asakura. Radiation forces on a dielectric sphere in the rayleigh scattering regime. *Optics communications*, 124(5-6):529–541, 1996.

[5] Oliver Reich, Grégory David, Kıvanç Esat, and Ruth Signorell. Weighing picogram aerosol droplets with an optical balance. *Communications Physics*, 3(1):223, 2020.

[6] Christian Lieber, Stefanos Melekidis, Rainer Koch, and Hans-Joerg Bauer. Insights into the evaporation characteristics of saliva droplets and aerosols: Levitation experiments and numerical modeling. *Journal of aerosol science*, 154:105760, 2021.

[7] Aidan Rafferty, Benjamin Vennes, Alison Bain, and Thomas C Preston. Optical trapping and light scattering in atmospheric aerosol science. *Physical Chemistry Chemical Physics*, 25(10):7066–7089, 2023.

[8] Giorgio Volpe and Giovanni Volpe. Simulation of a brownian particle in an optical trap. *American Journal of Physics*, 81(3):224–230, 2013.

[9] Patricia Daukantas. When optical tweezers met biology. *Optics and Photonics News*, 33(3):40–47, 2022.

[10] Malte Junk, Jörn Hinrichs, Fritz Polt, Jonas Fechner, and Werner Pauer. Quantitative experimental determination of evaporation influencing factors in single droplet levitation. *International Journal of Heat and Mass Transfer*, 149:119057, 2020.

[11] Javier Tello Marmolejo, Adriana Canales, Dag Hanstorp, and Ricardo Méndez-Fragoso. Fano combs in the directional mie scattering of a water droplet. *Physical Review Letters*, 130(4):043804, 2023.

[12] A Michelson, Simon Newcomb, AA Michelson, A Graham Bell, Reingold, and S Tolansky. Introduction to interferometry, 1880.

[13] Gustav Mie. Beiträge zur optik trüber medien, speziell kolloidaler metallösungen. *Annalen der physik*, 330(3):377–445, 1908.

[14] Georgia State University. Nave, Carl R. Thin lens equation, http://hyperphysics.phy-astr.gsu.edu/hbase/geoopt/lenseq.html, visited 17.04.2023, 2015.

[15] Jan Gieseler, Juan Ruben Gomez-Solano, Alessandro Magazzù, Isaac Pérez Castillo, Laura Pérez García, Marta Gironella-Torrent, Xavier Viader-Godoy, Felix Ritort, Giuseppe Pesce, Alejandro V Arzola, et al. Optical tweezers—from calibration to applications: a tutorial. *Advances in Optics and Photonics*, 13(1):74–241, 2021.

[16] PDP90A 2D Lateral Effect Position Sensor User Guide. https://www.thorlabs.com/thorproduct.cfm?partnumber=pdp90a.

[17] Thomas Young. Ii. the bakerian lecture. on the theory of light and colours. *Philosophical transactions of the Royal Society of London*, (92):12–48, 1802.

[18] A Ashkin and JM Dziedzic. Observation of resonances in the radiation pressure on dielectric spheres. *Physical Review Letters*, 38(23):1351, 1977.

[19] A Mazolli, PA Maia Neto, and HM Nussenzveig. Theory of trapping forces in optical tweezers. *Proceedings of the Royal Society of London. Series A: Mathematical, Physical and Engineering Sciences*, 459(2040):3021–3041, 2003.

[20] Mikhail F Limonov, Mikhail V Rybin, Alexander N Poddubny, and Yuri S Kivshar. Fano resonances in photonics. *Nature Photonics*, 11(9):543–554, 2017.